Structure and Mechanical Properties of Electroplated Mossy Lithium: Effects of Current Density and Electrolyte

Yikai Wang[a], Dingying Dang[a], Xingcheng Xiao[b], and Yang-Tse Cheng[a,*]*

[a] Department of Chemical and Materials Engineering, University of Kentucky, Lexington, KY 40506, USA.

[b] Chemical and Materials Systems, General Motors Global Research and Development Center, Warren, MI 48090, USA.

AUTHOR INFORMATION

Corresponding Author

* E-mail: ywa286@g.uky.edu; yang.t.cheng@uky.edu

Keywords: Lithium metal electrode, mechanical behavior, size effect, porosity, creep

The authors declare no competing financial interest.

Acknowledgments

This work is supported by the Vehicle Technologies Office of the U.S. Department of Energy Battery Materials Research (BMR) Program under Contract Number DE-EE0007787 and the National Science Foundation Award No. 1355438. The work performed at the University of Kentucky was also supported by Mercedes-Benz Research & Development North America, Inc. The authors would like to thank Tobias Glossmann and Stephen J. Harris for helpful discussions.

Structure and Mechanical Properties of Electroplated Mossy Lithium: Effects of Current Density and Electrolyte

ABSTRACT

Mechanical suppression, *e.g.*, by applying stack pressures and using functionalized coatings, has been considered a promising approach to inhibit the formation of lithium (Li) dendrites and improve the cycling stability of the Li metal electrode. However, a lack of understanding of the mechanical behavior of electroplated mossy Li, consisting of loosely packed Li dendrites that are covered by solid electrolyte interphase, hinders the development of mechanical suppression strategies and limits the understanding of the electromechanical behavior of mossy Li. In this study, we investigated, using flat punch indentation in an argon-filled glovebox, the room temperature mechanical behavior and its relationship with the microstructure of mossy Li electroplated using different current densities (between 0.25 and 10 mA/cm^2) in several electrolytes. The dendrite size decreases and the porosity of mossy Li increases with increasing current density. Mossy Li has lower Young's modulus (E) but significantly higher creep resistance than bulk Li. A scaling relationship between E and porosity is established for mossy Li. The creep behavior of mossy Li exhibits a strong size effect, *i.e.*, the steady-state impression velocity decreases with decreasing dendrite size. These findings provide a comprehensive understanding of the relationship between the microstructure and mechanical behavior of mossy Li.

Keywords: Lithium metal electrode, mechanical behavior, size effect, porosity, creep

The increasing demand for long-driving range electric vehicles has stimulated intensive search for high capacity electrodes. Lithium (Li) metal, with a theoretical capacity of 3862 mAh/g and the lowest reduction voltage (-3.04 V *vs.* the standard hydrogen electrode), has been considered one of the most promising anodes for high energy density rechargeable batteries. However, Li metal electrodes are prone to uncontrollable growth of Li dendrites and mossy Li during repeated plating/stripping cycling. The fragile mossy Li can be broken during cycling, forming electronically isolated "dead" lithium [1-3]. In liquid electrolyte-based Li metal batteries, the spontaneous formation of solid electrolyte interphase (SEI) on the surface of Li dendrites continuously and irreversibly consumes the electrolyte and Li [4]. Both factors lead to the low Coulombic efficiency (CE) of Li metal electrodes.

To improve the cycling stability of Li metal electrodes, extensive attempts have been made to develop new electrolytes (both solid and liquid forms) [5, 6], electrolyte additives [7-9], and host structures [10-12] to inhibit the formation of Li dendrites. Alternatively, mechanical suppression, by applying an external pressure or depositing coatings (e.g., artificial SEIs), can help maintain the structural and electronic connection of mossy Li and, as shown by recent studies [3, 13-16], improve the cycling stability of Li metal electrodes. For example, a 90 % CE of Li metal electrodes in a Li||Cu pouch cell can be sustained for over 120 cycles at 1 mA/cm^2 under an externally applied pressure of 1.1 MPa, while the CE is almost zero after 100 cycles in cells without the external pressure [14]. Developing mechanical suppression approaches thus requires the understanding of the mechanical behavior of bulk and mossy Li [17-22]. Recently, the elasticity, plasticity, time-dependent behavior, temperature-dependent deformation, and size effect of bulk and pristine Li have been investigated by various mechanical characterization approaches, including uniaxial tensile [23-26], compression [23, 25, 27], indentation [26, 28-32], and micropillar compression [33], in protective environment. More recently, it was found that mossy Li from electrochemical cycling could have a dramatically different mechanical behavior from bulk Li [28]. Unsurprisingly, therefore, mechanical suppression methods, based only on the mechanical properties of bulk and pristine Li, are not always effective [34-36]. To better inform the design of mechanical suppression approaches, it is necessary to gain a comprehensive understanding of the mechanical behavior of mossy Li and its relationship with the microstructure, such as dendrite size, porosity, and SEI, since all of which are effected by the current density and electrolyte.

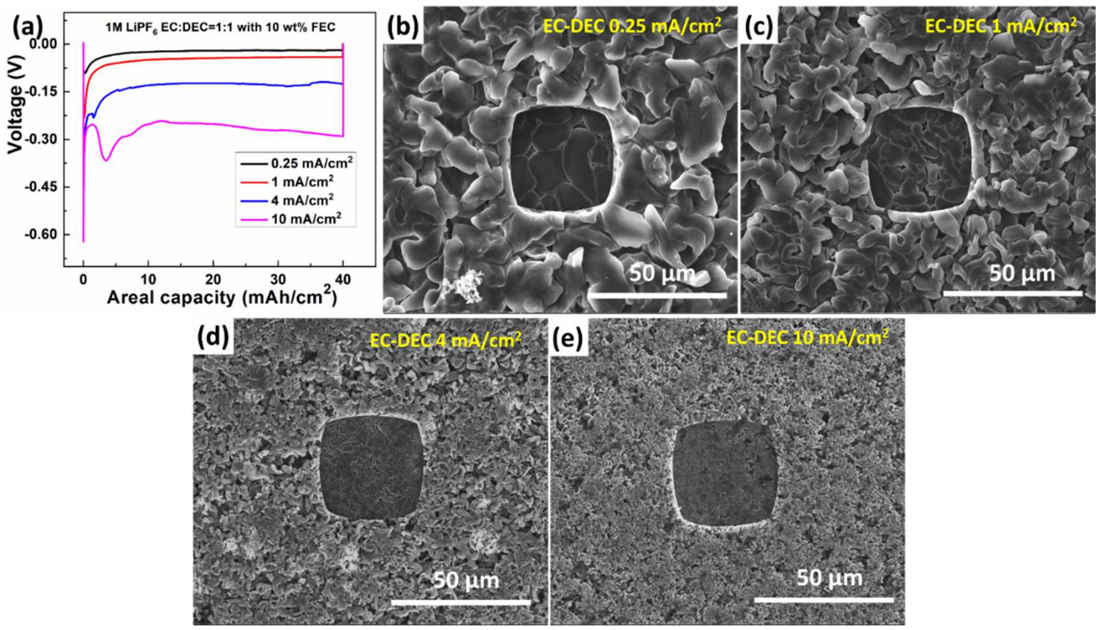

Fig. 1. (a) The voltage *vs.* areal capacity profiles of Li||Li symmetric cells with the EC-DEC electrolyte. (b)-(e) are the surface morphology and indents in the mossy Li electroplated at (b) 0.25 mA/cm^2, (c) 1 mA/cm^2, (d) 4 mA/cm^2, and (e) 10 mA/cm^2, respectively, in the EC-DEC electrolyte.

In this study, we investigated the mechanical behavior and microstructure of electroplated mossy Li obtained at different current densities (in the range between 0.25 to 10 mA/cm^2) in several electrolytes using flat punch indentation measurements in an argon-filled glovebox [28, 32]. The advantages of the flat punch over other indenters are (1) the flat punch indenter has a constant contact area and (2) its measurements are less sensitive to surface roughness and randomly distributed pores on the surface of mossy Li. Three typical liquid electrolytes were used, including the ethylene carbonate-diethyl carbonate (EC-DEC) electrolyte (1M $LiPF_6$ in EC : DEC = 1:1 with 10 wt.% fluoroethylene carbonate), 1,3-dioxolane-1,2-dimethoxyethane (DOL-DME) electrolyte (0.4 M LiTFSI and 0.6 M $LiNO_3$ in DOL-DME), and 4 M LiFSI in DME. Li plating was conducted in Li||Li Swagelok cells (with an external pressure of about 0.113 MPa) to avoid damaging the mossy Li during the cell disassembling process [28]. The areal capacity for Li plating of all Li||Li cells is 40 mAh/cm^2.

Fig. 1a shows the voltage profiles of the Li||Li cells during electroplating using the EC-DEC electrolyte. Each voltage profile consists of a spike and a plateau. The voltage spike is caused by the nucleation of Li dendrites on the plating side [37, 38]. As nucleation proceeds, dendrite growth dominates the electroplating of Li, which has a lower overpotential than that during nucleation. The voltage spike therefore decreases gradually. On the stripping side, the dissolution of Li gradually roughens the surface (which is covered by a native oxide layer), forming “pits” [38]. Due to the low charge transfer and mass transfer resistances of fresh Li inside the “pits,” Li preferentially strips from “pits” instead of the smooth surface [38, 39]. This is another factor for the continuous decrease of voltage in the initial electroplating. When nucleation is suppressed and dendrite growth becomes stable, particularly at low current densities (e.g., 0.25 and 1 mAh/cm^2), the voltage profile gradually becomes a plateau. At 10 mAh/cm^2, the overpotential in the plateau region is higher than the spike at 0.25 mAh/cm^2 (Fig. S1a), implying that dendrite nucleation may be active in the plateau region at 10 mAh/cm^2. Perturbations in the highly tortuous and thick mossy structure obtained at high current densities (shown later by the cross-sectional SEM images) may affect the balance between nucleation and dendrite growth and cause the fluctuations in the voltage profiles at high current densities in the plateau region, as shown in Fig. 1a and Fig. S1.

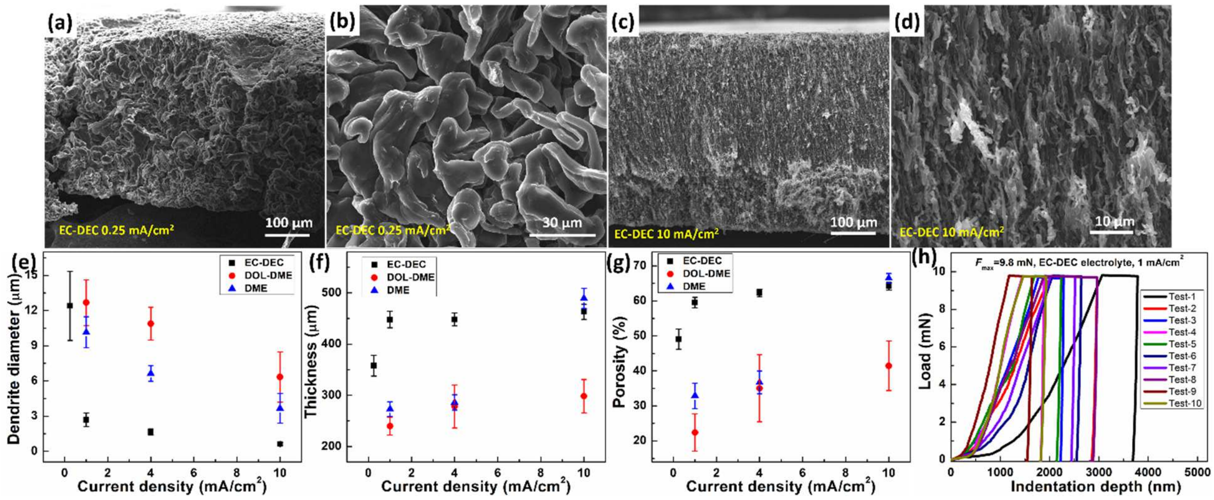

Fig. 2. The cross-sectional microstructure of mossy Li electroplated at (a)-(b) 0.25 mA/cm^2 and (c)-(d) 10 mA/cm^2. (e)-(g) are the variation of the average dendrite diameter, thickness, and porosity of mossy Li with the current density, respectively. (h) shows the typical flat punch indentation L-D curves (with F_{max} = 9.8 mN) of mossy Li obtained at 1 mA/cm^2 in the EC-DEC electrolytes.

The magnitude of both spike and plateau increases with increasing current density, as shown in Fig. S1. The voltage plateau at 10 mA/cm^2 is even larger than the spikes at low current densities (0.25 and 1 mA/cm^2), indicating that (1) more nucleation events happen at high current densities and (2) dendrites are prone to grow at low current densities, as confirmed by the dendrite morphology in the surface and cross-sectional images (Fig. 1b-e, Fig. 2a-d, and Fig. S2). As shown in Fig. 2e, the average diameter of Li dendrites increases from 0.62 to 12.41 μm as the current density decreases from 10 to 0.25 mA/cm^2 in the EC-DEC electrolyte. Li dendrites formed at high current densities (*e.g.*, 4 and 10 mA/cm^2) align vertically and have a high aspect ratio, while dendrites formed at low current densities, *e.g.*, 1 and 0.25 mA/cm^2, are oriented randomly with a low aspect ratio (Fig. 2a-d and Fig. S2). In addition, the average thickness of mossy Li increases with increasing current density (Fig. 2f). The average porosity of mossy Li is derived from the relationship among the areal capacity, density of Li, thickness of mossy Li, and the irreversible loss of Li ions caused by forming SEI (detailed in Supplementary material). As the current density increases from 0.25 to 10 mA/cm^2, the average porosity increases from 49.1 % to 64.2 % (Fig. 2g). Similar relationships among the voltage profiles, dendrite morphology, and current density were also found in the Li||Li cells with the DOL-DME and DEM electrolytes, as shown in Fig. S1, S3, and S4. At the same current density, the size of dendrites in different electrolytes follows the sequence: EC-DEC < DME < DOL-DME, while the thickness and porosity of mossy Li follow the opposite trend.

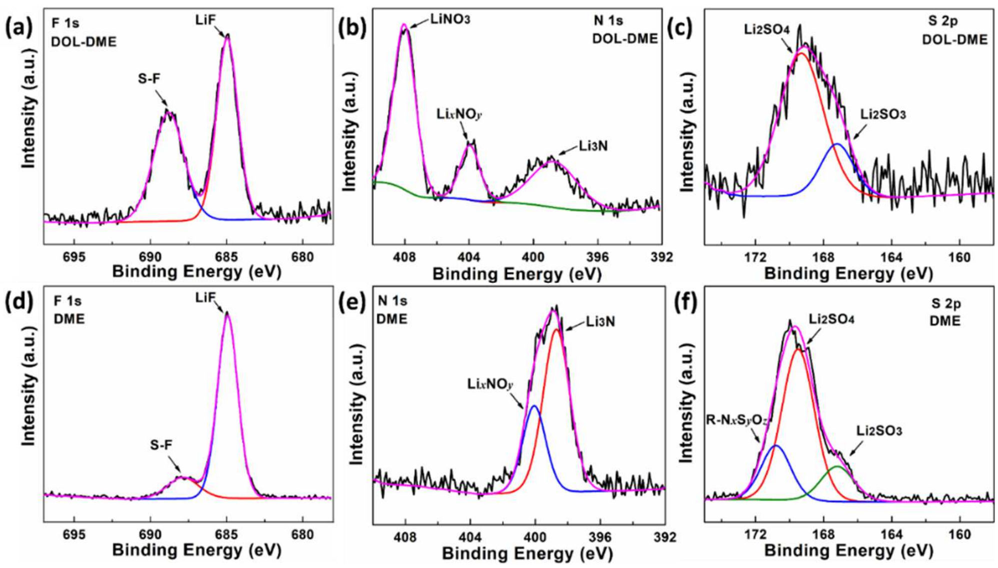

Fig. 3. X-ray photoelectron spectroscopy (XPS) of F 1s, N 1s, and S 2p of mossy Li electroplated in the DOL-DME and DME electrolytes. The XPS spectra of mossy Li electroplated in the EC-DEC electrolyte can be found in our recent study [28].

In addition, the composition of SEI depends on the electrolyte. The major inorganic components in the SEIs are (1) LiF, Li_2CO_3, Li_2O, LiOH, and Li_xPF_y on the dendrites electroplated in the EC-DEC electrolyte [28] and (2) LiF, Li_3N, Li_2O, Li_2SO_4, and Li_xNO_y on the dendrites electroplated in the DOL-DME and DME electrolytes, as shown in Fig. 3 and Refs. [40-42].

As shown in Fig. 1b-e and Fig. S3, the flat punch can cover several dendrites and thus measures the average mechanical behavior of mossy Li. Fig. 2h and Fig. S6 show that the load-displacement (L-D) curves of mossy Li using the same loading/unloading rate and the maximum load (F_{max}) are location-dependent due to the random nature of surface roughness and pore distribution [28]. The indentation depth (h_{in}) increases with the load during the loading process, keeps increasing during the holding period, and elastically recovers by tens of nanometers during unloading. The small recovery of h_{in} upon unloading shows that the elastic deformation is negligible compared to the plastic deformation and creep of mossy Li. Since the thickness of mossy Li is larger than 10 times of the maximum indentation depth (h_{max} < 20 μm), we did not consider the substrate effect on the indentation measurements. The small frictional force (< 5 % of F_{max}) between the side-face of the flat punch indenter and the mossy Li was also neglected in analyzing indentation data [28]. In this paper, error bars represent the standard deviation of multiple measurements.

The Young's modulus of mossy Li (E_{mossy}) are deduced from the unloading and holding data of flat punch indentation measurements using the approach detailed in Ref. [28]. E_{mossy} is the average modulus of the moss structure instead of individual dendrites. As shown in Table S2, the average E of mossy Li distributes in the range between 0.5 and 3.5 GPa, which is smaller than that (~7.8 GPa) of bulk Li. The E value of mossy Li electroplated in the EC-DEC electrolyte increases with decreasing current density. Statistically, E does not show a clear dependence on F_{max} and h_{max} (Fig. 4a, b and Fig. S7) despite that mossy Li was densified more by a larger F_{max} and h_{max}. We averaged the value of E measured with different F_{max} for mossy Li electroplated at each current density and established a relationship, analogous to the Gibson-Ashby scaling equation [43], between the average Young's modulus (E_{ave}) and porosity (p_{mossy}) of mossy Li,

$$E_{ave} = CE_d(1 - p_{mossy})^n \quad (1)$$

where C and n are fitting parameters, E_d is the theoretical Young's modulus of individual Li dendrites. For cellular foams, n=1 is for stretch-dominated and n=2 is for bending-dominated deformation behavior [44]. Equation (1) has been widely adapted for scaling mechanical properties of various porous metallic materials, such as nanoporous gold [45-47], despite that C may not equal to 1 to satisfy the condition that $E_{ave}/E_d = 1$ when $p_{mossy} = 0$.

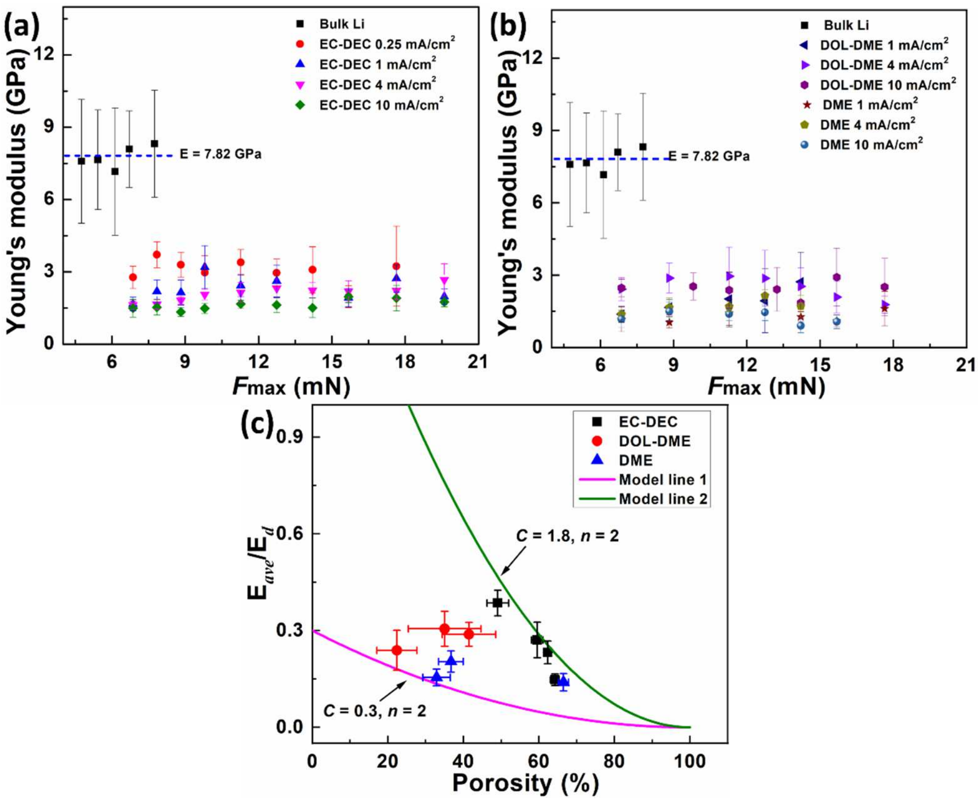

Fig. 4. (a) and (b) are the Young's modulus *vs.* F_{max} profiles of electroplated mossy Li. (c) The E_{ave}/E_d *vs.* p_{mossy} profiles of mossy Li and the modeling lines by Eq. (1).

Since the electroplated Li dendrites have a core-shell structure with Li as the core and SEI as the shell (Fig. S8a) [40, 48, 49], we may estimate E_d using [45, 50],

$$E_d = \frac{V_{Li}}{V_{dendrite}} E_{Li} + \frac{V_{SEI}}{V_{dendrite}} E_{SEI} \tag{2}$$

where V_{Li}, V_{SEI}, and $V_{dendrite}$ are the volume of Li, SEI, and the dendrite, respectively. $V_{dendrite} = V_{Li} + V_{SEI}$. For simplification, we assumed the E of all SEIs as 58.5 GPa [51] since the major inorganic SEI components have similar E values (Table S3). The SEIs on Li dendrites electroplated in the EC-DEC, DOL-DME, and DME electrolytes are assumed to have a thickness of 10, 20, and 20 nm [40, 48], respectively, although the thickness of SEI may differ with the current density. As shown in Table S4, E_d is larger than the Young's modulus of bulk Li due to the high modulus of the SEIs. The smaller E of mossy Li than bulk Li (~7.8 GPa) is, therefore, caused by the compliance of the porous microstructure.

Based on Equation (1) and (2), the E_{ave}/E_d *vs.* p_{mossy} profiles of mossy Li were plotted in Fig. 4c. The effect of electrolytes on the elasticity of mossy Li is shown clearly by the different E_{ave}/E_d *vs.* p_{mossy} profiles of mossy Li electroplated at the same current density. Here, we use Equation (1) with $n = 2$ (assuming that dendrites can bend under the flat punch) to fit the E_{ave}/E_d *vs.* p_{mossy} profiles. We found that all the data points fall in the region defined by $C = 1.8, n = 2$ and $C = 0.3, n = 2$. Conversely, E of mossy Li electroplated under other conditions may be evaluated by Equation (1) and (2) using appropriate values of C and n.

The increasing indentation depth during the holding period is caused by creep. As shown in Fig. 5a and Fig. S9a, the indentation creep depth (h_{creep}) of mossy Li during the holding period increases with increasing punching stress ($\sigma_{ind} = F_{max}/A$, where A is the projected area of the flat punch). h_{creep} corresponding to the same F_{max} generally increases with decreasing current density.

Using the approach detailed in Refs. [28, 52], we determined the steady-state impression velocity (v_{sind}) as the expectation value of the Gaussian distribution of the impression velocity (v_c) in the holding period between 400 and 600 s, when v_c trends to be constant (Fig. 5b, c, and Fig. S9b). Under the same σ_{ind}, v_{sind} of mossy Li electroplated in the same electrolyte increases with decreasing current density, as shown in Fig. 5d and Fig. S9c.

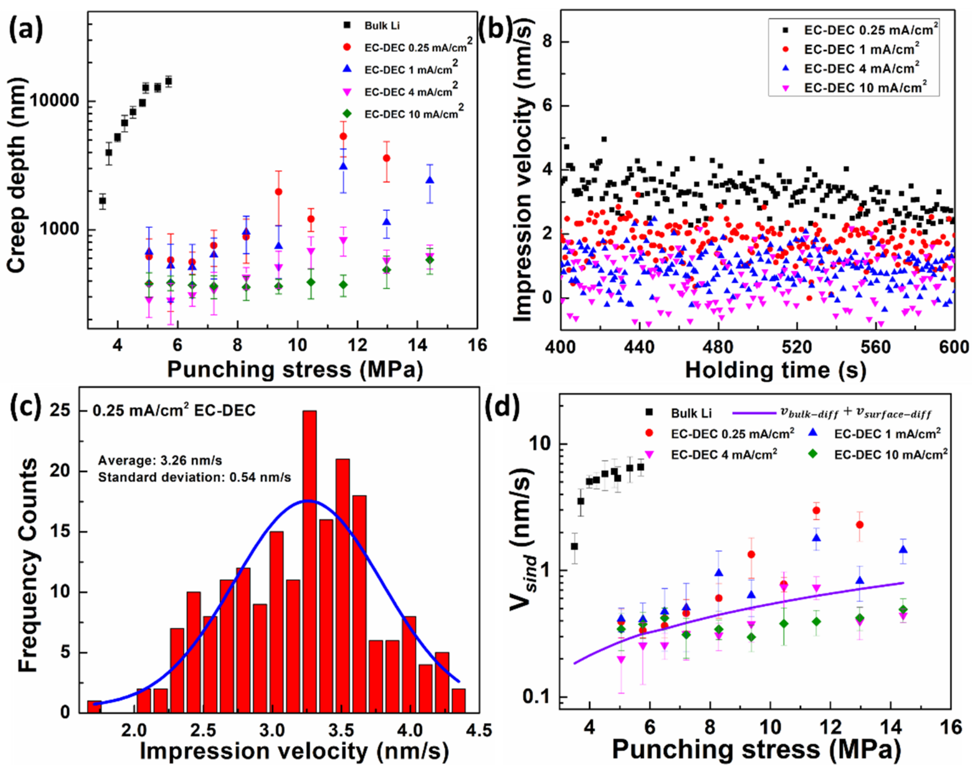

Fig. 5. (a) The creep depth *vs.* punching stress profiles of mossy Li (electroplated in the EC-DEC electrolyte) and bulk Li. (b) The impression velocity of mossy Li during the holding period between 400 and 600 s. The maximum load is 15.68 mN. (c) A typical Gaussian distribution of the impression velocity of mossy Li with F_{max} = 15.68 mN. (d) The steady-state impression velocity of mossy and bulk Li under different punching stresses. The steady-state impression velocity of mossy Li electroplated in the DOL-DME and DME electrolytes can be found in the Supplementary material. $v_{bulk-diff}$ represents the

impression velocity caused by bulk diffusion and $v_{surface-diff}$ represents the impression velocity caused by surface diffusion (or interface diffusion) at the interface between Li and the flat punch [52].

Despite its high porosity, mossy Li has much smaller h_{creep} and v_{sind} than bulk Li measured at the same F_{max}. The high v_{sind} of bulk Li is attributed to dislocation-mediated creep mechanisms, particularly diffusion-assisted dislocation climb due to its high homologous temperature (~0.66) at room temperature (RT) [23, 24, 53]. In contrast, the dislocation starvation or dislocation multiplication-induced entanglements in micro-sized Li dendrites increases the driving force for the nucleation or motion of dislocations [33]. As a result, the dislocation-mediated creep mechanisms are inhibited in mossy Li. Our recent study showed that v_{sind} of the mossy Li electroplated at 4 mA/cm^2 in the EC-DEC electrolyte is close to that caused by bulk- and surface-diffusion (*i.e.*, $v_{bulk-diff} + v_{surface-diff}$ [28]). As the current density decreases, the dendrite size increases. The probability of activating a dislocation source in individual dendrites increases as the stressed volume increases [54]. As a result, the maximum punching stress that the mossy structure can sustain decreases, the size effect weakens, and the creep of mossy Li becomes "bulk-like," *i.e.*, dislocation-mediated mechanisms contribute more to the creep behavior. Consequently, the creep resistance of mossy Li decreases with decreasing current density.

On the other hand, the inorganic SEI components mainly consist of ionic crystalline compounds, such as LiF and LiOH. These ionic crystals with high melting points (> 450 °C) creep slowly by diffusion-controlled mechanisms at RT under the stress level between several and tens of MPa [55]. For example, the creep strain rate of LiF at a high temperature (650 and 300 °C) is much smaller than that of Li metal at RT (Table S5) [56, 57]. Therefore, the ionic components in SEI are highly creep-resistant and can enhance the creep resistance of mossy Li at RT. As estimated by the core-shell structure model of Li dendrites (Fig. 8a, Eq. (S2), and (S3)), the volume ratio of SEI in mossy Li increases with increasing current density (Fig. S8b). This may be another reason for the increasing creep resistance of mossy Li as the current density increases. Similar to the effects of absorbed oxygen layers and artificial coatings on the deformation behavior of nanoporous gold [45, 58], SEI may also inhibit the dislocation nucleation on dendrite surface, suppress the dislocation-mediated creep, and impede the creep deformation of mossy Li. Overall, the enhanced creep resistance of mossy Li is a combined effect of the dendrite size and SEI. Future efforts are needed to distinguish the respective roles of these two factors.

The porosity in structural materials can usually increase the compliance and promote creep. Although the mossy Li electroplated at a larger current density has a higher porosity than that obtained at a lower current density, the former has greater creep resistance. Therefore, the size effect and SEI have a greater influence on creep than porosity in electroplated mossy Li.

The mechanical properties of mossy Li are important for developing dendrite suppression strategies, particularly selecting proper stack pressures, to improve the cycling stability of Li metal electrodes in liquid electrolyte-based batteries. The poor electrical connection among dendrites has been considered a major cause for the low CE of Li metal electrodes [3, 14, 16, 49]. Applying a proper stack pressure, which induces structural collapse and densifies the porous mossy structure, is a facile and economic approach to re-build and maintain electronic connections between "dead" mossy Li and the conductive network or hosts. For example, many "dead" Li chunks remain on the stripping side of the Li||Li Swagelok cell under a low pressure of 0.05 MPa after 8 cycles (Fig. S10a and b). The erratic voltage profile (Fig. S10c) of the cell implies the formation of many fractal-like dendrites [59], which can easily cause short-circuit. In contrast, no residual Li dendrites or chunks were found on the stripping side of the Li||Li cell under a pressure of 0.113 MPa after 8 cycles and the voltage profiles are normal U-shaped and n-shaped curves during cycling (Fig.

S10c-e). Moreover, the thickness of the mossy Li on the plating side of the cell under a pressure of 0.05 MPa is about 79.6 μm, larger than that (~ 63.4 μm) of the cell under a pressure of 0.113 MPa, as shown in Fig. S11. These observations show clearly the impact of stack pressure on the cycling stability of Li metal electrodes. However, the best stack pressure for Li metal electrodes is still unknown. In general, stack pressure should be selected by considering (1) the mechanical properties and accommodated volume changes of mossy Li, cathode, and polymeric separators, (2) the internal stress induced by the plating/stripping of mossy Li [60], (3) the microstructure changes of mossy Li during long-term plating/stripping cycling [38, 61], (4) temperature [16, 62, 63], and (5) safety hazard since a high pressure may drive Li dendrites to pierce through separator and cause short circuit.

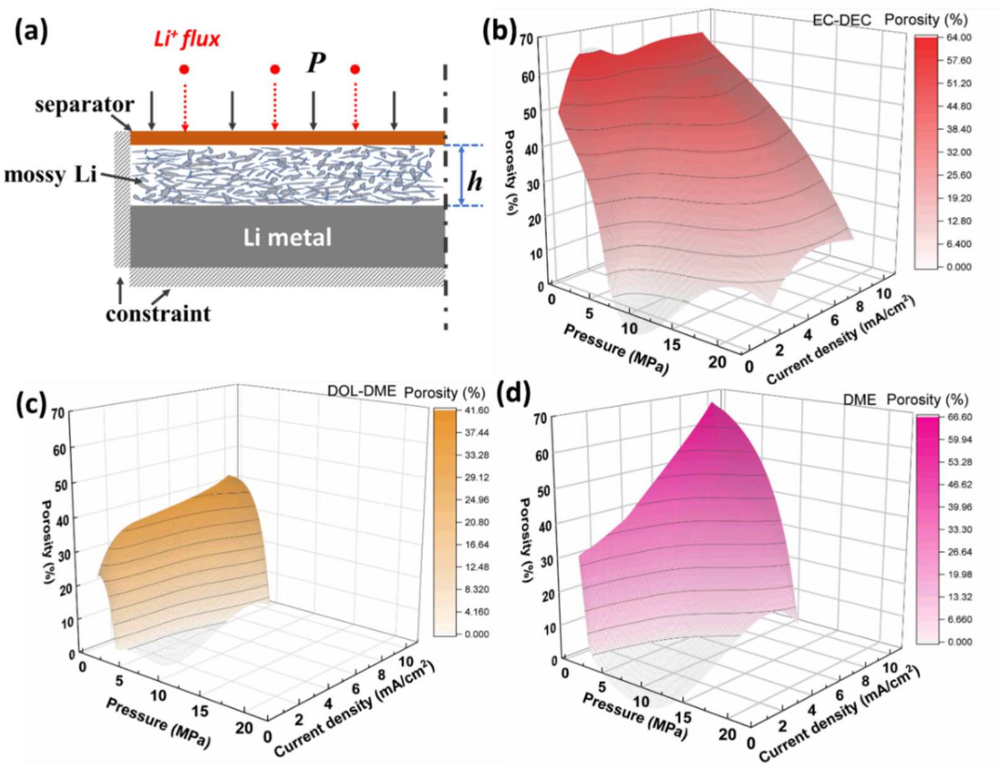

Fig. 6. (a) A schematic diagram of Li plating under a stack pressure of *P*. The bottom and the lateral side are constrained. The mossy Li can only be electroplated between the Li metal electrode and separator. (b)-

(d) show the porosity profiles of mossy Li as a function of the current density and stack pressure in the EC-DEC, DOL-DME, and DME electrolytes at RT, respectively.

In a simplified model shown in Fig. 6a, we assume that (1) mossy Li is uniformly electroplated between the separator and the bulk Li electrode in the vertical direction and (2) deformation of the separator and bulk Li during electroplating does not change during electroplating. At a current density of J, the mossy Li layer grows at a rate of $\dot{h}$,

$$\dot{h}(P,\ J) = \frac{J}{Q_{Li}\rho_{Li}(1-p_P)} \tag{3}$$

where p_P is the porosity of mossy Li electroplated under a stack pressure of P. When $P = 0$,

$$\dot{h}(P = 0,\ J) = \frac{J}{Q_{Li}\rho_{Li}(1-p_0)} \tag{4}$$

$$\dot{h}(P,\ J) = \dot{h}(P = 0,\ J) - v_{sind}(P,J) \tag{5}$$

where p_0 is the porosity of mossy Li electroplated without stack pressure which may be calculated by the thickness and the estimated v_{sind} of mossy Li at 0.113 MPa (Table S6). Q_{Li} and ρ_{Li} are the specific capacity and density of Li, respectively. $v_{sind}(P,J)$ designates its P and J (J determines the average dendrite size). Based on Equation (3)-(5), we mapped the relationship among the porosity of mossy Li, pressure, and current density during electroplating with different electrolytes in Fig. 6b-d, which may facilitate the selection of proper stack pressure for Li metal electrodes. For example, if a porosity of 25 % can prevent the electronic isolation of mossy Li, the stack pressure should be at least 4.3 and 15.5 MPa, respectively, for the current density of 0.25 and 10 mA/cm^2 in the EC-DEC electrolyte. To render mossy Li the same porosity, one should increase the stack pressure with increasing current density, which is consistent with the increasing tendency of v_{sind} with increasing dendrite size.

In conclusion, the current density and electrolyte have vital effects on the microstructure (*e.g.*, the dendrite size and porosity) and mechanical properties of mossy Li. In the same electrolyte, mossy Li electroplated at a higher current density has smaller dendrite size but larger porosity than that electroplated at a lower current density. At the same current density, the size of dendrites in mossy Li follows the sequence: EC-DEC < DME < DOL-DME, while the porosity of mossy Li shows an opposite tendency. E of mossy Li can be correlated with the porosity and properties of SEI by a scaling relationship. Although mossy Li has lower E than bulk Li, its creep resistance is remarkably higher than that of bulk Li. v_{sind} of mossy Li decreases with increasing current density due to the dendrite size-dependent creep mechanisms and the strengthening effect of SEI. Based on the creep behavior of mossy Li, we mapped the porosity profiles of mossy Li as a function of the current density and external pressure during electroplating to help select the proper stack pressure for Li metal electrodes. The mechanical behavior of mossy Li, which is distinct from that of bulk Li, is critical for the design of mechanical suppression approaches for Li metal electrodes and provides useful input parameters for electromechanical modeling of mossy Li. In addition, the environmental flat punch indentation method, as demonstrated in this study, can be used to study the mechanical behavior of other mossy-like metallic electrode materials (such as sodium, potassium, and zinc) towards eliminating their electrochemical cycling instability.

Supplementary material

Experimental procedure, more L-D curves and SEM images, and analysis results can be found in the Supplementary material.

Acknowledgments

This work is supported by the Vehicle Technologies Office of the U.S. Department of Energy Battery Materials Research (BMR) Program under Contract Number DE-EE0007787 and the National Science Foundation Award No. 1355438. The work performed at the University of Kentucky was also supported by Mercedes-Benz Research & Development North America, Inc. The authors would like to thank Tobias Glossmann and Stephen J. Harris for helpful discussions.

References

[1] W. Xu, J. Wang, F. Ding, X. Chen, E. Nasybulin, Y. Zhang, J.-G. Zhang, Energy & Environmental Science, 7 (2014) 513-537.
[2] D. Lin, Y. Liu, Y. Cui, Nature nanotechnology, 12 (2017) 194.
[3] J. Zheng, T. Tang, Q. Zhao, X. Liu, Y. Deng, L.A. Archer, ACS Energy Letters, (2019).
[4] D. Aurbach, E. Zinigrad, Y. Cohen, H.J.S.s.i. Teller, 148 (2002) 405-416.
[5] J. Qian, W.A. Henderson, W. Xu, P. Bhattacharya, M. Engelhard, O. Borodin, J.-G. Zhang, Nature communications, 6 (2015) 6362.
[6] L. Suo, Y.-S. Hu, H. Li, M. Armand, L. Chen, Nature communications, 4 (2013) 1481.
[7] J. Zheng, M.H. Engelhard, D. Mei, S. Jiao, B.J. Polzin, J.-G. Zhang, W. Xu, Nature Energy, 2 (2017) 17012.
[8] H. Zhang, G.G. Eshetu, X. Judez, C. Li, L.M. Rodriguez ‐ Martínez, M. Armand, Angewandte Chemie International Edition, 57 (2018) 15002-15027.
[9] Y. Ma, Z. Zhou, C. Li, L. Wang, Y. Wang, X. Cheng, P. Zuo, C. Du, H. Huo, Y. Gao, Energy Storage Materials, 11 (2018) 197-204.
[10] D. Lin, J. Zhao, J. Sun, H. Yao, Y. Liu, K. Yan, Y. Cui, Proceedings of the National Academy of Sciences, 114 (2017) 4613-4618.
[11] J. Pu, J. Li, K. Zhang, T. Zhang, C. Li, H. Ma, J. Zhu, P.V. Braun, J. Lu, H. Zhang, Nature communications, 10 (2019) 1896.
[12] Y. Tang, K. Shen, Z. Lv, X. Xu, G. Hou, H. Cao, L. Wu, G. Zheng, Y. Deng, Journal of Power Sources, 403 (2018) 82-89.
[13] Y. Zhao, G. Li, Y. Gao, D. Wang, Q. Huang, D. Wang, ACS Energy Letters, (2019).
[14] X. Yin, W. Tang, K.C. Phua, S. Adams, S.W. Lee, G.W. Zheng, Nano energy, 50 (2018) 659-664.
[15] Y. Liu, Y.-K. Tzeng, D. Lin, A. Pei, H. Lu, N.A. Melosh, Z.-X. Shen, S. Chu, Y. Cui, Joule, 2 (2018) 1595-1609.
[16] M. Genovese, A. Louli, R. Weber, C. Martin, T. Taskovic, J. Dahn, Journal of The Electrochemical Society, 166 (2019) A3342-A3347.
[17] C. Monroe, J. Newman, Journal of The Electrochemical Society, 152 (2005) A396-A404.
[18] C. Monroe, J. Newman, Journal of The Electrochemical Society, 151 (2004) A880-A886.
[19] L. Anand, S. Narayan, Journal of The Electrochemical Society, 166 (2019) A1092-A1095.
[20] S. Narayan, L. Anand, Extreme Mechanics Letters, 24 (2018) 21-29.
[21] P. Wang, W. Qu, W.L. Song, H. Chen, R. Chen, D. Fang, Advanced Functional Materials, (2019) 1900950.

[22] X. Zhang, Q.J. Wang, K.L. Harrison, K. Jungjohann, B.L. Boyce, S.A. Roberts, P.M. Attia, S.J. Harris, Journal of The Electrochemical Society, 166 (2019) A3639-A3652.
[23] A. Masias, N. Felten, R. Garcia-Mendez, J. Wolfenstine, J. Sakamoto, Journal of Materials Science, 54 (2019) 2585-2600.
[24] W.S. LePage, Y. Chen, E. Kazyak, K.-H. Chen, A.J. Sanchez, A. Poli, E.M. Arruda, M. Thouless, N.P. Dasgupta, Journal of The Electrochemical Society, 166 (2019) A89-A97.
[25] S. Tariq, K. Ammigan, P. Hurh, R. Schultz, P. Liu, J. Shang, in: Proceedings of the 2003 particle accelerator conference, IEEE, 2003, pp. 1452-1454.
[26] C.D. Fincher, D. Ojeda, Y. Zhang, G.M. Pharr, M. Pharr, Acta Materialia, (2019).
[27] R.P. Schultz, in, Fermi National Accelerator Lab., Batavia, IL (US), 2002.
[28] Y. Wang, D. Dang, M. Wang, X. Xiao, Y.-T. Cheng, Applied Physics Letters, 115 (2019) 043903.
[29] E.G. Herbert, S.A. Hackney, V. Thole, N.J. Dudney, P.S. Phani, Journal of Materials Research, 33 (2018) 1361-1368.
[30] E.G. Herbert, S.A. Hackney, V. Thole, N.J. Dudney, P.S. Phani, Journal of Materials Research, 33 (2018) 1347-1360.
[31] E.G. Herbert, S.A. Hackney, N.J. Dudney, P.S. Phani, Journal of Materials Research, 33 (2018) 1335-1346.
[32] Y. Wang, Y.-T. Cheng, Scripta Materialia, 130 (2017) 191-195.
[33] C. Xu, Z. Ahmad, A. Aryanfar, V. Viswanathan, J.R. Greer, Proceedings of the National Academy of Sciences, 114 (2017) 57-61.
[34] Y. Ren, Y. Shen, Y. Lin, C.-W. Nan, Electrochemistry Communications, 57 (2015) 27-30.
[35] Q. Li, T. Yi, X. Wang, H. Pan, B. Quan, T. Liang, X. Guo, X. Yu, H. Wang, X. Huang, Nano Energy, 63 (2019) 103895.
[36] L. Porz, T. Swamy, B.W. Sheldon, D. Rettenwander, T. Frömling, H.L. Thaman, S. Berendts, R. Uecker, W.C. Carter, Y.M. Chiang, Advanced Energy Materials, 7 (2017) 1701003.
[37] A. Pei, G. Zheng, F. Shi, Y. Li, Y. Cui, Nano letters, 17 (2017) 1132-1139.
[38] K.N. Wood, E. Kazyak, A.F. Chadwick, K.-H. Chen, J.-G. Zhang, K. Thornton, N.P. Dasgupta, ACS central science, 2 (2016) 790-801.
[39] F. Shi, A. Pei, D.T. Boyle, J. Xie, X. Yu, X. Zhang, Y. Cui, Proceedings of the National Academy of Sciences, 115 (2018) 8529-8534.
[40] J. Wang, W. Huang, A. Pei, Y. Li, F. Shi, X. Yu, Y. Cui, Nature Energy, 4 (2019) 664-670.
[41] X.B. Cheng, R. Zhang, C.Z. Zhao, F. Wei, J.G. Zhang, Q. Zhang, Advanced Science, 3 (2016) 1500213.
[42] J. Qian, B.D. Adams, J. Zheng, W. Xu, W.A. Henderson, J. Wang, M.E. Bowden, S. Xu, J. Hu, J.G. Zhang, Advanced Functional Materials, 26 (2016) 7094-7102.
[43] L.J. Gibson, M.F. Ashby, Cellular solids: structure and properties, Cambridge university press, 1999.
[44] M. Ashby, Y. Bréchet, Acta materialia, 51 (2003) 5801-5821.
[45] M.M. Biener, J. Biener, A. Wichmann, A. Wittstock, T.F. Baumann, M. Bäumer, A.V. Hamza, Nano letters, 11 (2011) 3085-3090.
[46] E.-J. Gwak, H. Jeon, E. Song, N.-R. Kang, J.-Y. Kim, Acta Materialia, 155 (2018) 253-261.
[47] D.R. Gomes, A.A. Turkin, D.I. Vainchtein, J.T.M. De Hosson, Scripta Materialia, 164 (2019) 17-20.
[48] Y. Li, Y. Li, A. Pei, K. Yan, Y. Sun, C.-L. Wu, L.-M. Joubert, R. Chin, A.L. Koh, Y. Yu, Science, 358 (2017) 506-510.

[49] C. Fang, J. Li, M. Zhang, Y. Zhang, F. Yang, J.Z. Lee, M.-H. Lee, J. Alvarado, M.A. Schroeder, Y. Yang, Nature, 572 (2019) 511-515.
[50] X. Liu, J. Hu, B. Pan, Physica E: Low-dimensional Systems and Nanostructures, 40 (2008) 3042-3048.
[51] Q. Zhang, X. Xiao, W. Zhou, Y.T. Cheng, M.W. Verbrugge, Advanced Energy Materials, 5 (2015) 1401398.
[52] S. Chu, J. Li, Journal of Materials Science, 12 (1977) 2200-2208.
[53] P. Sargent, M. Ashby, Scripta metallurgica, 18 (1984) 145-150.
[54] E.G. Herbert, N.J. Dudney, M. Rochow, V. Thole, S.A. Hackney, Journal of Materials Research, 34 (2019) 3593-3616.
[55] W.R. Cannon, T.G. Langdon, Journal of Materials Science, 18 (1983) 1-50.
[56] C.N. Rao, A. Ruoff, Journal of Applied Physics, 43 (1972) 1437-1440.
[57] D.R. Cropper, T.G. Langdon, Philosophical Magazine, 18 (1968) 1181-1192.
[58] P. Wu, X.-L. Ye, L.-Z. Liu, H.-J. Jin, Materials Research Letters, 6 (2018) 508-514.
[59] K.N. Wood, M. Noked, N.P. Dasgupta, ACS Energy Letters, 2 (2017) 664-672.
[60] J.H. Cho, X. Xiao, K. Guo, Y. Liu, H. Gao, B.W. Sheldon, Energy Storage Materials, (2019).
[61] Y. Zhang, F.M. Heim, N. Song, J.L. Bartlett, X. Li, ACS Energy Letters, 2 (2017) 2696-2705.
[62] C.T. Love, O.A. Baturina, K.E. Swider-Lyons, ECS Electrochemistry Letters, 4 (2015) A24-A27.
[63] C.T. Love, Journal of Electrochemical Energy Conversion and Storage, 13 (2016) 031004.

Graphical Abstracts